

Article

Adsorption Kinetics of Imidacloprid, Acetamiprid and Methomyl Pesticides in Aqueous Solution onto Eucalyptus Woodchip Derived Biochar

Assadawoot Srikhaow ¹, Wasitthi Chaengsawang ¹, Tanongkiat Kiatsiriroat ², Puangrat Kajitvichyanukul ^{3,4,*} and Siwaporn M. Smith ^{1,*}

¹ Center of Sustainable Energy and Green Materials and Department of Chemistry, Faculty of Science, Mahidol University, 999 Phuttamonthon Sai 4 Road, Salaya 73170, Thailand; assadawoot.sri@gmail.com (A.S.); cw.wasitthi@gmail.com (W.C.)

² Department of Mechanical Engineering, Faculty of Engineering, Chiang Mai University, 239 Huay Kaew Road, Muang District, Chiang Mai 50200, Thailand; tanong@dome.eng.cmu.ac.th

³ Department of Environmental Engineering, Faculty of Engineering, Chiang Mai University, 239 Huay Kaew Road, Muang District, Chiang Mai 50200, Thailand

⁴ Sustainable Engineering Research Center for Pollution and Environmental Management, Faculty of Engineering, Chiang Mai University, 239 Huay Kaew Road, Muang District, Chiang Mai 50200, Thailand

* Correspondence: puangrat.k@cmu.ac.th (P.K.); siwaporn.smi@mahidol.edu (S.M.S.); Tel.: +66-61-6598715 (P.K.); +66-93-5939449 (S.M.S.)



Citation: Srikhaow, A.; Chaengsawang, W.; Kiatsiriroat, T.; Kajitvichyanukul, P.; Smith, S.M. Adsorption Kinetics of Imidacloprid, Acetamiprid and Methomyl Pesticides in Aqueous Solution onto Eucalyptus Woodchip Derived Biochar. *Minerals* **2022**, *12*, 528. <https://doi.org/10.3390/min12050528>

Academic Editors: Susan T. L. Harrison, Anna H. Kaksonen and Keiko Sasaki

Received: 11 January 2022

Accepted: 18 April 2022

Published: 24 April 2022

Publisher's Note: MDPI stays neutral with regard to jurisdictional claims in published maps and institutional affiliations.



Copyright: © 2022 by the authors. Licensee MDPI, Basel, Switzerland. This article is an open access article distributed under the terms and conditions of the Creative Commons Attribution (CC BY) license (<https://creativecommons.org/licenses/by/4.0/>).

Abstract: This work reports the application of a biochar (BC) derived from eucalyptus wood chips to remove pesticides (imidacloprid, acetamiprid and methomyl) from water. The pseudo-second order kinetic adsorption model is the best fit describing the adsorption of pesticides on BC. Furthermore, the Langmuir model correlated well with the adsorption isotherm data for acetamiprid and methomyl, while the Freundlich model was selected to explain the adsorption of imidacloprid on BC. The maximum adsorption capacities for methomyl, imidacloprid and acetamiprid on the BC material are 32.42, 14.75 and 4.87 mg g⁻¹, respectively. The highest adsorption capacity of methomyl on the BC surface could be the result of multilayer adsorption suggested by the adsorption isotherm studies, with imidacloprid (or acetamiprid) monolayer being adsorbed on the BC surface. The structure, functional groups of pesticides, including their polarity, all played an important role contributing to the performance of biochar sorbent. Preferable interactions between the studied pesticides and the BC surface may include π - π interactions and hydrogen bonding. The steric aromatic entity in adsorbed imidacloprid and acetamiprid on the BC surface may hinder the possibility of other pesticide molecules approaching the available sorption sites on the surface.

Keywords: biochar; eucalyptus wood chips; pesticides contaminated water; sorption; methomyl; imidacloprid; acetamiprid

1. Introduction

Pesticides have been widely used to control unwanted pests, vector-borne diseases, and weeds in public spaces, agricultural fields, and private gardens. However, the long-term application of pesticides may leave toxic residues that may contaminate natural water bodies (ground and surface water) adjacent to the application areas through leaching, surface drainage, spray leftovers, spray drift and runoff [1]. The residual pesticides in water reservoirs can be accumulated in aquatic and marine organisms' food chain, raising human health risks and the negative impact to ecological systems [2].

Neonicotinoids and carbamate pesticides have been commonly used for agricultural and household activities. Being highly soluble in water [3,4] such pesticides have often been found in the environment, e.g., ground and surface water [4–6]. Based on their toxicity, neonicotinoids and carbamate pesticides are classified as Class II and Class III [7] for

neonicotinoids pesticides and Class I (restricted-use pesticide) for carbamate pesticides [8] by the United States Environmental Protection Agency (US EPA). Regulated by the EU and US EPA, the permissible concentrations of an individual pesticide in the ground and surface water should be in the limit of $0.1 \mu\text{g L}^{-1}$. If there are more than one pesticide, the total concentration of all pesticides should be equal to or below $0.5 \mu\text{g L}^{-1}$. Nevertheless, the concentrations of pesticide residue in ground water, surface water and soil were found to be much higher than the permissible level (ranging from several $\mu\text{g L}^{-1}$ to more than hundred $\mu\text{g L}^{-1}$), as shown in Table 1 [5,6,9–13]. The residual pesticides are not only toxic, but also highly persistent and, potentially bio-accumulative [14,15]. Hence, the removal of pesticides from water generally required advanced water purification technologies, i.e., biological oxidation, ozone and chemical oxidation, Fenton and Fenton coupled with photolysis, solid-phase extraction, advanced oxidation processes, membrane filtration, and adsorption. Several methods required complicated system setup which increased the cost and generated secondary, perhaps more toxic, contaminant products [16]. On the other hand, simple adsorption processes have been known as energy- and cost-efficient technologies without the requirement of advanced setup [17–19]. Hence, developments of low-cost and high-performance sorbents seemed to be the key to practical adsorption applications.

Table 1. Detection of acetamiprid, imidacloprid and methomyl pesticides in the environment.

Pesticides	Contamination Area	Concentration ($\mu\text{g L}^{-1}$)	References
Acetamiprid	Wetlands	Up to 225	[5]
Acetamiprid	Water reservoirs	Up to 7.7	[9]
Imidacloprid	Surface water	320	[6]
Imidacloprid	Surface water	Up to 3.29	[10]
Imidacloprid	Soil	Up to 60	[11]
Methomyl	Ground water	10	[12]
Methomyl	Strawberry farm canal	30	[13]

Sorbent productions from recycling and utilizing wood residues and agricultural wastes are economical solutions and sustainable alternatives for wastewater remediation by using low-cost, non-toxic, and naturally abundant starting materials. Biochar, a co-product from biomass pyrolysis in a closed system with limited oxygen supply, has recently been used as an efficient sorbent for the removal of organic pollutants in water such as dyes, pharmaceuticals, and pesticides [20]. Various types of agricultural wastes and wood, such as oak wood [21], rice straw [22], grape pomace [23], peanut fiber [24], coconut shell [25] and soybeans [26], have been utilized as raw parent materials for the production of low-cost biochar materials, which were used to decontaminate pesticides in wastewater. Note that eucalyptus is one of the most globally planted woods to supply the paper and furniture industry [27]. Undersized eucalyptus woodchip, including residues such as barks and leaves, may be applied as solid fuel, producing low-cost heat for boilers and steam turbines. With their plentiful amount, eucalyptus residues can be alternatively utilized as raw parent materials for biochar production, instead of burning all of them for generating heat and greenhouse gases (GHGs). Previous works reported the application of biochar-derived from eucalyptus residues for the treatment of wastewater containing heavy metal contaminants, such as U (VI) [28], Cr (VI) [29], As [30], Cd (II) [31], Ni(II) and Pb(II) [32]. Fernandes and coworkers utilized eucalyptus derived biochar to remove aqueous fluoxetine [33]. There have been a limited number of reports that demonstrated effective sorbents derived from eucalyptus residues. From the literature, a eucalyptus bark biochar sorbent was applied in the removal of atrazine or imidacloprid pesticides from water [22]. Additional reports on the adsorption capacity of pesticides over biochar produced from undersized eucalyptus woodchip should add more research input that could be used as evidence to promote the conversion of abundant biomass to high-value products and the circular economy business.

In this study, three pesticides (acetamiprid, imidacloprid, and methomyl) were employed, due to their extensive use, in a comparative adsorption study over a eucalyptus

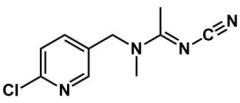
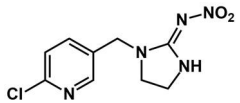
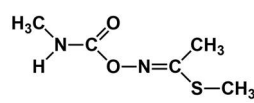
wood biochar sorbent. The adsorption experiments were systematically carried out in aqueous media to determine the optimal sorbent loading, adsorption kinetics, and isotherms, as well as the maximum adsorption capacities of pesticides on the biochar. The adsorption capacities are varied depending on the electrostatic interactions between the biochar surface and the pesticides' chemical entity. The isothermal adsorption behavior of each pesticide on the biochar surface, as well as the structure and polarity of pesticides, are key parameters linked to the performance of the biochar sorbent. Possible hydrogen bonding and π - π interactions between the investigated biochar material and pesticides are discussed, as well as the adsorption preferences of polar pesticides on the biochar surface.

2. Materials and Methods

2.1. Chemicals and Materials

Acetamiprid (Phoenix Rich, 20% w v⁻¹), imidacloprid (Saima chemical, 70%WG), and methomyl (HEBEI ENGE BIOTECH, 97%TC; 970 g kg⁻¹) are of commercial grade and are used as received without further purification. The structures and physical properties of pesticides studied are listed in Table 2. Double-distilled water was used as a solvent. Biochar (BC) and pyrolyzed eucalyptus woodchips were supplied by the Faculty of Engineering, Chiang Mai University, Thailand. Prior to use, the BC sample was dried, ground and sieved with a stainless-steel mesh size of 80 (particle size < 177 μ m).

Table 2. Characteristics of pesticides. ^a HA: Hydrogen bonding acceptor index; ^b HD: hydrogen bonding donor index.

Pesticide	Acetamiprid	Imidacloprid	Methomyl
Molecular formula	C ₁₀ H ₁₁ ClN ₄	C ₉ H ₁₀ ClN ₅ O ₂	C ₅ H ₁₀ N ₂ O ₂ S
Structure formula			
Log <i>K</i> _{ow}	0.80	0.57	0.60
p <i>K</i> _a	0.70	1.56, 11.12	13.27
Water solubility (g L ⁻¹)	4.2	0.610	57.9
HA ^a	4	4	4
HD ^b	0	1	1
Molecular weight (g mol ⁻¹)	222.7	255.7	162.2

2.2. BC Characterization

The chemical composition of BC (carbon C, nitrogen N, hydrogen H and sulfur S) was analyzed using a CNHS analyzer (LECO Corporation, CHNS 628, St. Joseph, MI, USA). A powder X-ray diffractometer (Bruker, D2 Phaser, Billerica, MA, USA), equipped with a Cu-K α radiation source, was used to identify crystalline phases in the BC material at diffraction angles (2-Theta) ranging from 10° to 80°. A Raman spectrometer (Horiba, XploRa Plus, Kyoto, Japan), operated with a 532 nm wavelength laser, was utilized to study the structural carbon components in the BC sample. The morphology of the BC and its corresponding elemental compositions was determined on a scanning electron microscope (SEM, Hitachi, SU800, Tokyo, Japan) equipped with energy dispersive X-ray spectroscopy. The BC sample was lightly deposited on a carbon tape, later being coated with Pt prior to SEM measurements. An Fourier-transform infrared (FTIR) spectrophotometer (Thermo Electron Corporation, Nicolet 6700, Madison, WI, USA) was employed to analyze the chemical composition of the BC sample using the KBr pellet method at a measured wavenumber between 680 and 4000 cm⁻¹. The Brunauer–Emmett–Teller (BET, Micromeritics, ASAP 2026, Micromeritics, Norcross, GA, USA) surface analysis, N₂ adsorption-desorption was performed at 77 K, while the sample was degassed for 12 h at 200 °C prior to the adsorption-desorption measurement.

2.3. Adsorption

Batch experiments were performed at 25 °C and a pH of 7, using a thermostat shaker at an agitation speed of 150 rpm. A certain mass of BC (0.5–5 g L⁻¹) was introduced to a polypropylene bottle filled with 200 mL of a 50 ppm pesticide (aq). Equilibrium studies were performed by shaking the suspension containing BC and pesticide for specific time intervals (maximum of 6 h). Then, the supernatants were separated by simple filtering through a cellulose acetate syringe filter with a pore size of 0.45 µm, and the equilibrium pesticide concentrations after adsorption with BC were determined. The same batch experiment was carried out for 12 h without BC in the system in order to confirm negligible removal of pesticides due to cohesion forces between the pesticide and the container. The pesticide removal efficiencies were measured in triplicates for each condition using the following protocol. Firstly, the UV-Vis absorption spectrum of each aqueous pesticide solution was recorded on a UV-Vis Spectrophotometer (Thermo Scientific, GENESYS 10S, Waltham, MA, USA), while aqueous acetamiprid, imidacloprid, and methomyl gave their λ_{max} as 246 nm, 270 nm, and 234 nm, respectively. The concentrations of the aqueous pesticide solutions before and after BC treatments were evaluated using the calibration relations of absorbance and concentration data after constructing a calibration curve based on the Lambert–Beer law. The removal efficiency of each pesticide by BC [25] was calculated from the following equation:

$$\text{Removal efficiency (\%)} = ((C_0 - C_e)/C_0) \times 100 \quad (1)$$

where C_0 and C_e are the initial and equilibrium concentration (ppm) of pesticide before and after adsorption, respectively.

The amount of pesticide adsorbed at equilibrium (q_e , mg g⁻¹) was calculated by Equation (2),

$$q_e = ((C_0 - C_e)/V)/m \quad (2)$$

where V is the volume of pesticide aqueous solution (L), and m is the weight of biochar (g).

2.4. Sorption Isotherms

Sorption equilibrium was performed at 25 °C with pesticide concentration ranging from 10 ppm to 200 ppm at sorbent dosages of 5 g L⁻¹ for acetamiprid and methomyl and 0.5 g L⁻¹ for imidacloprid. The experimental procedures were conducted similarly to the above batch experiments, except that the suspensions were agitated for 6 h to ensure that adsorption processes reached equilibria. Two-parameter isotherms, the Langmuir and Freundlich adsorption models and three-parameter adsorption isotherm models, Sips and Redlich–Peterson, were used to examine the adsorption behavior of the pesticide on the biochar surface. Notably, the Langmuir isotherm can be used to describe adsorption processes based on the assumption that the adsorption process occurs at the specific homogeneous sites on the surface of the sorbent, implying that it is a monolayer adsorption [34]. The equation of the Langmuir isotherm is described as follows:

$$q_e = (q_{max} K_L C_e)/(1 + K_L C_e) \quad (3)$$

where C_e is the equilibrium concentration (ppm); q_e is the amount of adsorbed pesticide per unit mass of sorbent at equilibrium (mg g⁻¹); q_{max} is the maximum adsorption capacity (mg g⁻¹); and K_L is the Langmuir isotherm constant (L m⁻¹) related to the adsorption energy.

In addition, the Freundlich isotherm is an empirical equation assuming that the adsorption process happens with the heterogeneous surface via a multilayer adsorption mechanism [35]. The Freundlich adsorption equation is given as follows:

$$q_e = K_F (C_e)^{1/n} \quad (4)$$

where K_F is the affinity coefficient (L mg⁻¹) and n is the Freundlich exponential coefficient.

On the other hand, the Sips model [36] (or Langmuir–Freundlich adsorption isotherm) was developed to overcome the disadvantage of the Freundlich model. At high and low adsorbate concentrations, the Sips isotherm approaches the Langmuir and Freundlich isotherms [37], respectively. The equation of the Sips isotherm is given below:

$$q_e = q_{max,s} K_s C_e^{n_s} / (1 + K_s C_e^{n_s}) \quad (5)$$

where K_s is the Sips isotherm model constant ($L \text{ mg}^{-1}$); $q_{max,s}$ is the Sips isotherm maximum adsorption capacity (mg g^{-1}), and n_s is the Sips isotherm model exponent. Likewise, the Redlich–Peterson isotherm model [38] is a combination of the Langmuir and Freundlich isotherms. The Redlich–Peterson equation can be described as in the following equation:

$$q_e = K_{RP} C_e / (1 + a_{RP} C_e^\beta) \quad (6)$$

where K_{RP} ($L \text{ g}^{-1}$) and a_{RP} ($L \text{ mg}^{-1}$) $^{-\beta}$ are Redlich–Peterson isotherm constants and β is the Redlich–Peterson isotherm exponent, which lies between 0 and 1.

3. Results and Discussion

3.1. Characterization of Eucalyptus Wood Biochar

Table 3 summarizes the bulk concentration of C, H, N and S elements in the eucalyptus woodchip derived biochar (BC), and its surface properties. The elemental analysis data suggested that the BC material contains a high carbon content (83.7%), which is consistent with the typical carbon content (75–87%) reported for the eucalyptus-derived biochar samples prepared under pyrolytic temperature ranging from 450 °C to 950 °C [39,40].

Table 3. Physiochemical characteristics of the eucalyptus wood-derived biochar. ^a BET specific surface area; ^b Total pore volume ($P/P_0 = 0.989$); ^c average pore diameter ($4V/A$ by BET).

C	Elemental Compositions (% wt.)				SSA ^a ($\text{m}^2 \text{ g}^{-1}$)	V_p ^b ($\text{cm}^3 \text{ g}^{-1}$)	D_p ^c (nm)
	H	N	S				
83.7 ± 0.02	1.73 ± 0.25	0.74 ± 0.01	0.04 ± 0.01	4.02 ± 0.01	0.0084	8.36	

The BET specific surface area of the BC sample is $4.02 \text{ m}^2 \text{ g}^{-1}$, which is quite comparable to those of poultry litter, green waste from plant pruning, grass, switchgrass, and tea waste-derived biochar ($<10 \text{ m}^2 \text{ g}^{-1}$) produced at the temperature range of 400–500 °C [41–45]. As seen in Figure 1a, the N_2 adsorption-desorption isotherm of the eucalyptus woodchip derived BC exhibits an open hysteresis loop at low p/p_0 [46]. According to the IUPAC classification, the N_2 adsorption/desorption plot belongs to type IV with a well-defined plateau and a type H1 hysteresis loop, suggesting that the BC has a rigid mesoporous structure [47] with an average pore diameter of 8.36 nm and a pore volume of $0.008 \text{ cm}^3 \text{ g}^{-1}$. Several works demonstrated that mesoporous biochar materials, though having low surface areas ($<10 \text{ m}^2 \text{ g}^{-1}$), were effective sorbents in the removal of various pesticides from water [43,48,49]. The SEM image (in Figure 1b) provides evidence of the porous solid structure in the carbonaceous skeleton, with a rough and irregular surface and remaining tube-like structures similar to its parent material (Figure 1b). From the microstructure, BC has a porous surface texture with pore sizes ranging from 2.06 to 3.38 μm in the same range as biochar derived from eucalyptus wood [32].

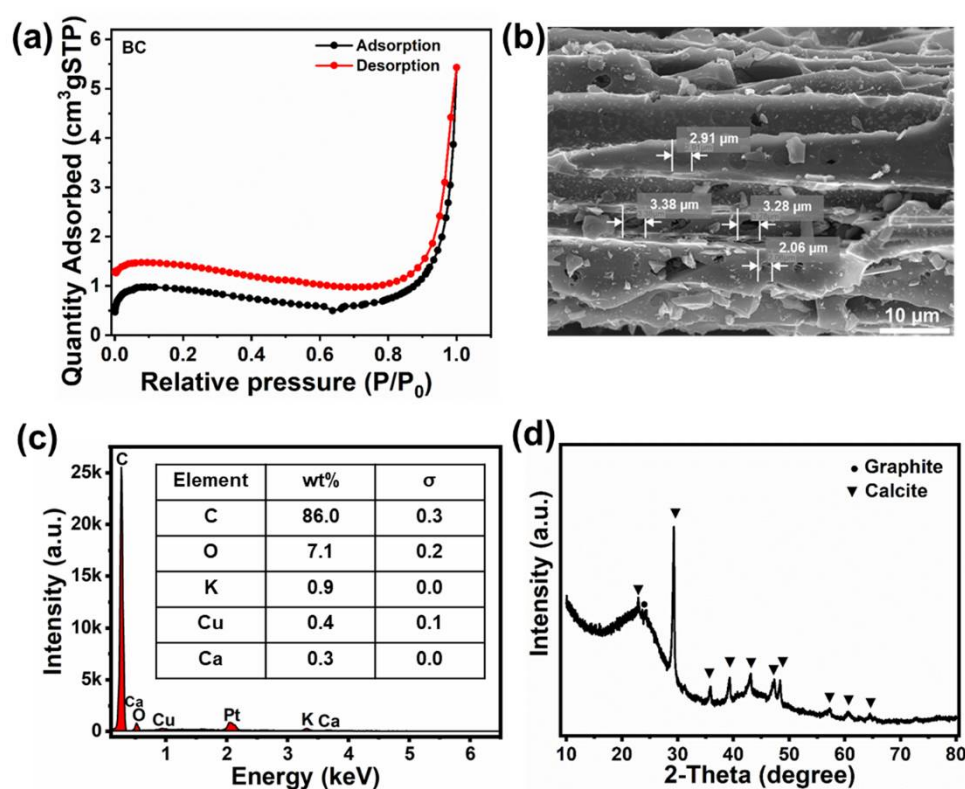


Figure 1. (a) N_2 adsorption-desorption isotherm of eucalyptus wood-derived biochar (BC), (b) SEM image and (c) corresponding EDX spectrum of the BC and (d) Powder XRD pattern of the BC. Note that, the observed Pt content found in (c) comes from the SEM coating.

Furthermore, energy dispersive X-ray (EDX) analyses (Figure 1c) indicate the carbon rich BC surface (86.0% wt.), being in excellent agreement with CNHS analysis data. Other minor elements found on the BC's surface include O (7.1%), K (0.9%), Cu (0.4%), and Ca (0.3%). Possible minerals in the BC samples are oxides and/or carbonates of potassium, copper and calcium originating from the eucalyptus woodchips. In the PXRD pattern of BC (Figure 1d) a broad peak with low intensity corresponds to amorphous carbon (23.0°), while sharp peaks are attributed mainly to the calcite ($CaCO_3$) phase, according to the Joint Committee on Powder Diffraction Standards (JCPDS) database [50]. No XRD peaks for other minerals such as oxides of K or Cu were observed, possibly due to the low crystallinity of other phases (if any) and the high background of amorphous carbon [51]. The small amount of Ca in the BC material and well-defined diffraction peaks corresponding to the calcite phase ($CaCO_3$) may imply that BC contains a trace amount of calcite with a sufficiently high crystallinity. The presence of calcite in biochar materials was previously reported when eucalyptus wood, corncob, pineapple peel [52], canola straw, corn straw, soybean straw and peanut straw [53] were used as feedstocks.

The Raman spectrum of the BC material in Figure 2a shows three typical peak related aromatic and graphitic hydrocarbons, so called D, G and 2D bands. The D band at $1300\text{--}1400\text{ cm}^{-1}$ attributed to the disorders or defects in the sp^2 structure of graphene originated from the formation of sp^3 carbon atoms because of the presence of amorphous carbon, heteroatoms, and vacancies [54]. The G band at $1500\text{--}1600\text{ cm}^{-1}$ is related to an ordered graphitic lattice of sp^2 carbon atoms, indicating a graphitic structure [55]. Additionally, the 2D band in the region of 2600 cm^{-1} referred to the second-order of the D band, which is characteristic of graphene structures [56] and its intensity frequently correlates with the number of material layers [57]. The obtained I_D/I_G intensity ratio of 0.71 indicated that the G band corresponding to graphitic structure was dominant, implying that the BC has a main proportion of ordered graphitic carbons. In Figure 2b, an intense IR peak at 3420 cm^{-1} is correlated to the stretching vibration of the OH groups in alcohol, phenol, and

carboxylic groups [58]. The peak at $2850\text{--}2920\text{ cm}^{-1}$ is attributed to aliphatic components (C-H, CH_2 or CH_3) of the hemicellulose and cellulose, whereas the IR peak at 1634 cm^{-1} corresponds to the aromatic carbon (C=C) and carbonyl (C=O) vibration in the carboxylic acid groups [59]. The vibrational bands at 1400 cm^{-1} and 870 cm^{-1} could be related to the O-C-O asymmetric stretching of carboxylate groups and aromatic C-H bending [60]. The presence of surface functional groups in BC, i.e., hydroxyl, phenolic, and carboxylic groups, can provide bonding sites for the adsorption of pollutants through a hydrogen bonding interaction [61]. It should provide a concise and precise description of the experimental results, their interpretation, as well as the experimental conclusions that can be drawn.

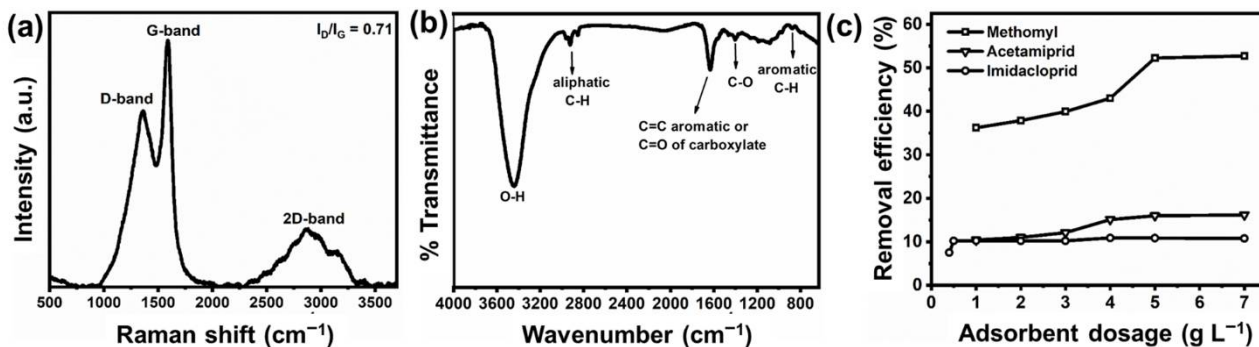


Figure 2. (a) Raman, (b) FTIR spectra of the BC. The D and G band in the Raman spectrum correlate to graphitic structures and defected graphitic structures, respectively, and (c) effect of adsorbent dosage on removal efficiencies of pesticides in an aqueous media (Conditions: 100 mL of aqueous solution of pesticide, $\text{pH} = 7$, $25\text{ }^\circ\text{C}$, 6 h).

3.2. Adsorption Test

3.2.1. Effect of Adsorbent Dosage

The optimal dosage of sorbent is an essential parameter for determining the adsorption capacity for a known initial concentration in a batch sorption experiment. The effect of BC sorbent dosage on sorption are illustrated in Figure 2c. The adsorbent dosage in this study was varied from 1 g L^{-1} to 7 g L^{-1} for methomyl and imidacloprid, while the adsorbent dosage for imidacloprid removal was varied from 0.4 g L^{-1} to 7 g L^{-1} . To ensure the adsorption process reached an equilibrium, the removal efficiencies of all pesticides were determined after 6 h of adsorption. Experimental results showed that the removal efficiencies increased slightly with increasing sorbent dosage, possibly due to an enhancement in adsorbent surface area and the availability of more sites for adsorption [62]. Interestingly, removal efficiencies for methomyl and acetamiprid reached the highest values of 52.29% and 16.00%, respectively, at an adsorbent loading of 5 g L^{-1} . However, the removal efficiencies of methomyl and acetamiprid were not significantly improved when the adsorbent loading was increased to 7 g L^{-1} . In contrast, the imidacloprid removal efficiency was 7.25% at a sorbent loading of 0.4 g L^{-1} , and it then reached 10.11% at a sorbent loading of 0.5 g L^{-1} . Similar to the above two pesticides, no significant improvement was found in the removal efficiency of imidacloprid when the adsorbent loading was increased up to $5\text{--}7\text{ g L}^{-1}$ (10–14 times of 0.5 g L^{-1}). The adsorption of the pesticides reached steady values after further increasing a higher amount of sorbent, possibly due to saturation coverage on the adsorption sites [63]. Thus, adsorbent loadings of 5 g L^{-1} for methomyl and acetamiprid and 0.5 g L^{-1} for imidacloprid were chosen to study the adsorption isotherms and adsorption kinetics of the pesticide removal in aqueous media by the BC material.

3.2.2. Adsorption Isotherm

From the adsorption isotherms in Figures 3 and 4, the equilibrium concentrations (C_e) of methomyl were found to be lower than the those from other pesticide treatments

due to the higher adsorption capacity of methomyl of the BC surface. Fitted curves of the adsorption isotherms computed by the two- and three parameter adsorption models, are included in Figures 3 and 4, respectively, whereas the information obtained from fitting the experimental data of pesticide adsorption is given in Table 4. In addition, the other two-parameter isotherms (Dubinin–Radushkevich and Temkin) were also tested and the fitted curves including the isotherm parameters are presented in Figure S1 and Table S1. Amongst two-parameter isotherm models, the Freundlich model provides a good description of imidacloprid adsorption with a higher correlation coefficient (R^2) of 0.9770 than that of the Langmuir model ($R^2 > 0.9750$). The results indicate that the BC has a heterogeneous distribution of surface energy for imidacloprid adsorption [64]. In contrast, the Langmuir isotherm ($R^2 > 0.975$) fits the experimental adsorption data of acetamiprid and methomyl better than the Freundlich isotherm according to the values of R^2 , suggesting the monolayer with the uniform heat of adsorption without interaction between the pesticide adsorbed molecules [65]. Furthermore, the maximum adsorption capacities calculated from the Langmuir model are 32.42, 14.75, and 4.78 mg g^{-1} for methomyl, imidacloprid and acetamiprid, respectively. Three-parameter isotherms, Sips and Redlich–Peterson, were also tested to amplify the R^2 and for their fittingness to explain the pesticide adsorption on BC.

The Redlich–Peterson model gave the highest R^2 for acetamiprid (0.9942) and methomyl (0.9940) adsorption, implying that it is the better fitting model. However, it is unable to simulate the adsorption behaviors because the values for β were greater than one for both acetamiprid and methomyl adsorption [66]. Thus, the Sips model was well-fitted to all pesticide adsorption data with R^2 values greater than 0.9900, suggesting the heterogeneous surface adsorption of pesticides on BC [36]. The value of n_s obtained from the Sips isotherm for methomyl adsorption was higher than one, suggesting that the Sips isotherm tended to resemble the Freundlich model. This indicates the multilayered adsorption of methomyl on the BC surface.

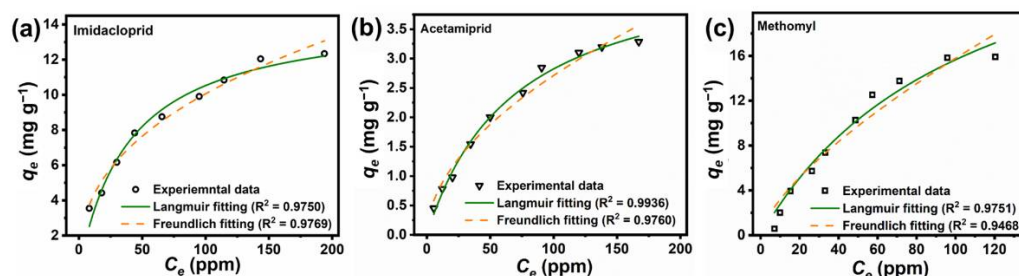


Figure 3. Two-parameter adsorption isotherms of (a) imidacloprid, (b) acetamiprid and (c) methomyl on the BC, respectively, by the Langmuir and Freundlich models. Conditions: 100 mL of aqueous solution of pesticide; initial concentrations = 10–200 ppm, pH = 7, 25 °C, 6 h.

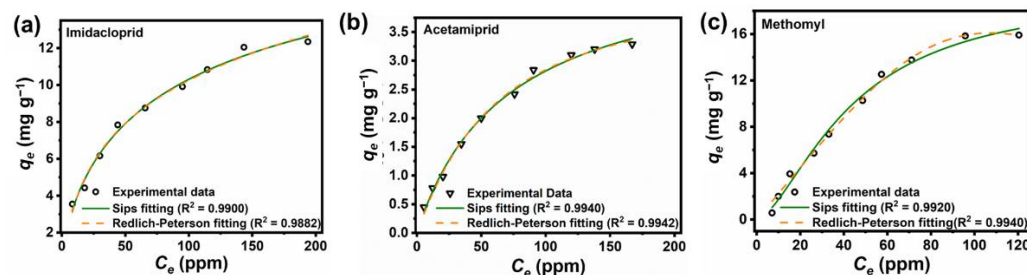


Figure 4. Three-parameter adsorption isotherms of (a) imidacloprid, (b) acetamiprid and (c) methomyl on the BC, respectively, by the Sips and Redlich–Peterson models. Conditions: 100 mL of aqueous solution of pesticide, pH = 7, 25 °C, 6 h.

Table 4. Parameter of adsorption isotherms for imidacloprid, acetamiprid and methomyl adsorption on BC.

	Models	Isotherm Parameters	Pesticides		
			Imidacloprid	Acetamiprid	Methomyl
Two-parameter	Langmuir	q_{max} (mg g ⁻¹)	14.75	4.78	32.42
		K_L (L mg ⁻¹)	0.0252	0.0014	0.0094
		R^2	0.9750	0.9936	0.9751
	Freundlich	K_F (L mg ⁻¹)	1.6274	0.2356	0.6432
		n	2.5783	1.8843	1.4391
		R^2	0.97	0.9760	0.9468
Three-parameter	Sips	$q_{m,s}$ (mg g ⁻¹)	21.07	4.87	19.78
		K_s (L mg ⁻¹)	0.0432	0.0149	0.0025
		n_s	0.6733	0.9836	1.5851
		R^2	0.9900	0.9940	0.9920
	Redlich and Peterson	K_{RP} (L g ⁻¹)	0.6988	0.0637	0.2250
		a_{RP} (L mg ⁻¹) ^{-β}	0.1677	0.0081	4.1 × 10 ⁻⁷
		$β$	0.7697	1.0934	2.9979
		R^2	0.9882	0.9942	0.9940

In contrast, the n_s values from the Sips isotherm for imidacloprid and acetamiprid are close to one, indicating that the adsorption behavior of imidacloprid and acetamiprid on BC dominantly occurs through monolayer adsorption. Thus, it is clearly seen that the Sips model gave the best fit of the experimental data based on the appropriate constants and correlation coefficients, possibly due to its ability to predict wide ranges of adsorbate concentration [36].

3.2.3. Adsorption Kinetics

The adsorption kinetics of pesticide adsorption on the BC material were studied using the initial pesticide concentration of 50 ppm at 25 °C, sorbent dosages of 5 g L⁻¹ (acetamiprid and methomyl) and 0.5 g L⁻¹ (imidacloprid). Notably, as seen in Figure 2c, it is unnecessary to use a high BC dosage for imidacloprid adsorption. The kinetics of methomyl, imidacloprid, and acetamiprid adsorption on the eucalyptus wood-derived BC (Figure 5) showed that adsorption of the pesticides rapidly occurred during the first 0.5 h, 2 h, and 3 h of adsorption for removal of imidacloprid, acetamiprid, and methomyl, respectively, and were subsequently followed by a slower rate until equilibrium was reached (at about 1 h for imidacloprid and 6 h for acetamiprid and methomyl). The fast adsorption at the initial stage possibly resulted from the large amount of unoccupied active sites on the biochar's surface and the strong interaction force between pesticide molecules and the surface functional groups of the sorbent [67]. The saturation of active sites and weak interaction force possibly led to the sorption equilibrium after the adsorption process was continuously carried out. To better understand the mechanism of pesticides adsorbed on the BC, three non-linear kinetic models, namely pseudo-first order, pseudo-second order, and Elovich, were applied to analyze the experimental data from the batch experiments.

Pseudo-first order (PFO) is given in Equation (7).

$$q_t = q_e (1 - e^{-kt}) \quad (7)$$

Pseud-second order (PSO) is given as:

$$q_t = (k_2 q_e^2 t) / (1 + (k_2 q_e t)) \quad (8)$$

where k_1 (h^{-1}) is the PFO adsorption rate constant, k_2 ($\text{g} (\text{mg h})^{-1}$) is the PSO rate constant, q_e and q_t (mg g^{-1}) are the amount adsorbed at equilibrium and the amount adsorbed at time “t”, respectively [68,69].

The Elovich model can be described as in Equation (9).

$$q_t = (1/\beta)\ln(1 + \alpha\beta t) \tag{9}$$

where α is the initial adsorption rate of pesticide ($\text{mg} (\text{g h})^{-1}$), and β is the desorption constant (g mg^{-1}) [70].

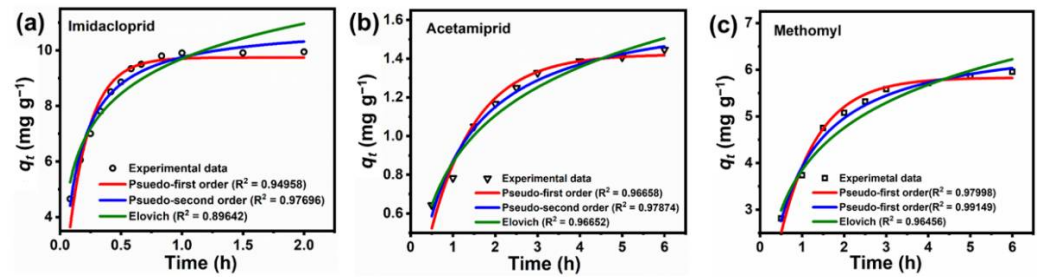


Figure 5. Adsorption kinetics of (a) imidacloprid, (b) acetamiprid and (c) methomyl on BC, respectively, by fitting pseudo-first order, pseudo-second order and Elovich models.

The calculated constants of the three kinetic equations and the correlation coefficient (R^2) values under adsorption experiments with three different pesticides are presented in Table 5. The R^2 and the similarity of the experimental adsorption capacity ($q_{e,exp}$) compared to the calculated adsorption capacity ($q_{e,cal}$) obtained by the kinetic models are typically used to determine the validity of the kinetic models. As seen in Table 5, the PSO kinetic model with the highest R^2 values (0.98–0.99) can more correctly describe the adsorption process of the three pesticides on the BC, and the calculated adsorption capacities ($q_{e,cal}$) for the PSO model matched well with the experimental adsorption capacities ($q_{e,exp}$). Thus, the adsorption mechanism of pesticides on BC in this study was possibly predominated by chemisorption [71]. The higher α values compared with β constants from the Elovich model in the adsorption of imidacloprid, acetamiprid, and methomyl indicated the higher rate of adsorption than desorption, suggesting the viability of pesticide adsorption on the BC [70].

Table 5. Kinetic parameters of the PFO, PSO and Elovich models for adsorption of imidacloprid, acetamiprid and methomyl on the eucalyptus wood-derived biochar. $q_{e,exp}$: experimental adsorption capacity and $q_{e,cal}$: calculated adsorption capacity (mg g^{-1}).

Pesticides	$q_{e,exp}$	PFO Model			PSO Model			Elovich Model		
		$q_{e,cal}$	k_1 (h^{-1})	R^2	$q_{e,cal}$	k_2 ($\text{g} (\text{mg h})^{-1}$)	R^2	α ($\text{mg} (\text{g h})^{-1}$)	β (g mg^{-1})	R^2
Imidacloprid	10.01	9.74	5.6075	0.9495	10.95	0.73912	0.9791	3.66×10^2	0.5468	0.8964
Acetamiprid	1.46	1.42	0.9167	0.9666	1.49	0.6251	0.9787	3.38	2.6609	0.9666
Methomyl	5.96	5.83	1.1147	0.9800	6.06	0.2034	0.9915	21.59	0.7333	0.9645

3.2.4. Adsorption Rate-Controlling Mechanism

The adsorption-rate-control mechanism of pesticides on the BC was studied by using the liquid film-diffusion (LFD) model, Equation (10), and the intra-particle diffusion (IPD) model, Equation (11).

$$qt = k_{ipd} \cdot t^{1/2} + C \tag{10}$$

$$\ln(1 - F) = -k_{lfd} \cdot t \tag{11}$$

where

$$F = q_t/q_e \quad (12)$$

k_{ipd} is the rate constant of the IPD model ($\text{mg g}^{-1} \text{h}^{0.5}$), C is the concentration (mg g^{-1}) which corresponds to the boundary layer thickness and k_{lfd} is the equilibrium fractional attainment (h^{-1}) [72,73].

The liquid film-diffusion and intra-particle diffusion modeling of the experimental data are shown in Figure 6a,b, and the calculated parameters are summarized in Table 6. As seen in Figure 6a, the non-linear relationship between q_t and $t^{1/2}$ was observed in IPD modeling in all pesticide adsorption systems, and the fitting curves did not pass through the origin. It indicates that several processes may be controlling the pesticide adsorption in this study [67]. Furthermore, R^2 values for the liquid film-diffusion model were higher than those for the intra-particle diffusion model. It indicates that film diffusion is the main rate-limiting step and contribution to external surface adsorption or instantaneous adsorption of pesticides [74]. The high C values suggested a large thickness of the film diffusion layers, possibly indicating the higher adsorption capability of imidacloprid and methomyl than that of acetamiprid on the BC sorbent.

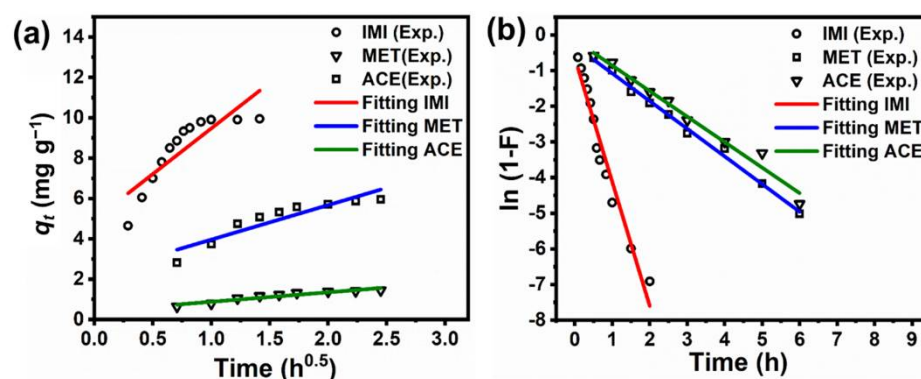


Figure 6. (a) Intra-particle diffusion model and (b) liquid film diffusion model fitting for the adsorption of imidacloprid (IMI), methomyl (MET) and acetamiprid (ACE) on the BC material.

Table 6. The kinetic parameters of the LFD and IPD models for imidacloprid (IMI), acetamiprid (ACE) and methomyl (MET) adsorption on BC.

Pesticides	LFD Model		IPD Model		
	K_{lfd} (h^{-1})	R^2	k_{ipd} ($\text{mg g}^{-1} \text{h}^{0.5}$)	C (mg g^{-1})	R^2
Imidacloprid	3.447	0.9578	4.519	4.954	0.7365
Acetamiprid	0.715	0.9797	0.4702	0.041	0.8993
Methomyl	0.776	0.9941	1.710	2.253	0.8513

3.2.5. Adsorption Mechanism

As seen in Figure 7, the FTIR spectrum of the BC before adsorption showed the characteristic absorption peaks of OH (3420 cm^{-1}) and C=C, C=O (broad peak around 1600 cm^{-1}). After adsorption with pesticides, the relative peak intensities corresponding to C=C, C=O shifted to a higher wavenumber after the adsorption of methomyl and acetamiprid, whereas those peaks slightly switched to a lower wavenumber after the adsorption of imidacloprid.

K_{ow} values usually reflect the polarity of pesticides and high Log K_{ow} pesticides (low polarity) tend to be less soluble in water [78]. Thus, based on Log K_{ow} values (imidacloprid (0.57), methomyl (0.60) and acetamiprid (0.80)), acetamiprid should be preferably adsorbed on the BC surface, compared with imidacloprid and methomyl. However, adsorption test results showed that BC is an effective sorbent for the relatively polar pesticides (imida-

cloprid and methomyl), possibly due to the contribution of the density of polar moieties on the BC [79] surface. The presence of polar groups (hydroxyl and carboxyl groups) on BC (observed by FTIR) should promote adsorption of pesticides with high polarity being supported on the sorbent surface. Furthermore, the π - π interaction between the aromatic carbon of the BC and the pyridine rings of imidacloprid and acetamiprid molecules may block and hinder other molecules from accessing the binding site at the external surface of the BC, resulting in lower adsorption capacities than those of methomyl.

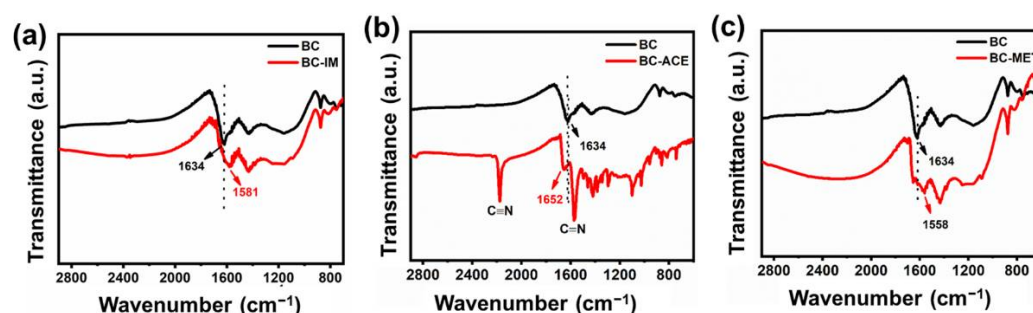
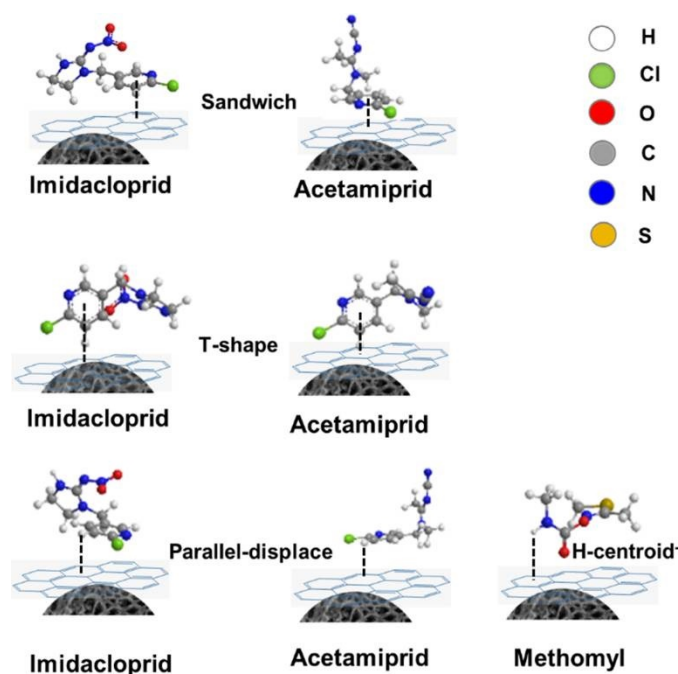
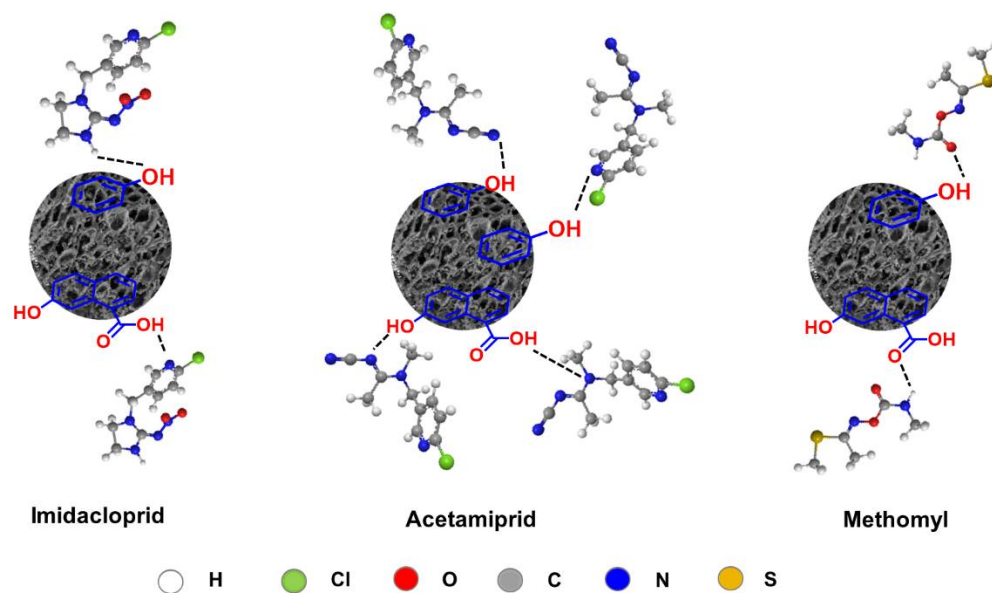


Figure 7. FTIR spectra of BC (black) and the spent BC samples (red) after treated with (a) imidacloprid (IM), (b) acetamiprid (ACE) and (c) methomyl (MET).

That may result from the interaction between aromatic derivatives present in the BC and pesticide molecules through the π - π interaction [75–77] formed between the pyridine rings (in imidacloprid and acetamiprid) and N-H (in methomyl), as proposed in Scheme 1. Another possible interaction is the OH (in alcohol, phenol, and carboxyl groups) and C=O (in carboxyl groups) on the BC surface interacting with the pesticide molecules by an H-bonding interaction, as illustrated in Scheme 2.



Scheme 1. Possible interaction between aromatic derivatives present in the BC and pesticide molecules through the π - π interaction.



Scheme 2. Possible interaction of the O-H and C=O on BC's surface interacting with the pesticide molecules by H-bonding.

3.2.6. Comparative Sorption Capacities of Pesticides on Various Sorbents

The adsorption capacities of three pesticides on BC from our study were compared with various adsorbents and they are reported in Table 7. The adsorption capacity of imidacloprid over BC is comparable to that of biochar derived from peanut shells, although the specific surface area of woodchip derived BC (in our study) is 130% smaller. Furthermore, the adsorption capacity of acetamiprid over BC is in the same range as that of bentonite and kaolin [80] clays.

Table 7. Langmuir adsorption capacities of the eucalyptus wood-derived biochar compared with previously reported carbon-based adsorbents from various raw parent materials.

Adsorbent	Pesticide	Temp. (°C)	Conc. Range (ppm)	Adsorption Capacity (mg g ⁻¹)	Surface Area (m ² g ⁻¹)	Adsorption Capacity per Surface Area (mg g ²)	Ref.
Eucalyptus wood	Imidacloprid	25	10–200	14.75	4.02	3.669	This work
Peanut shell	Imidacloprid	25	2.5–30	18.17	534.83	0.034	[81]
KOH-magnetic sugarcane bagasse	Imidacloprid	25	10–200	313.00	660	0.4742	[82]
KOH-magnetic corncob	Imidacloprid	25	10–200	410.00	192.30	2.1321	[83]
Eucalyptus wood	Acetamiprid	25	10–200	4.78	4.02	1.1891	This work
KOH-tangerine peel	Acetamiprid	25	0.01–1	37.51	697.80	0.038	[84]
FeCl ₃ -pistachio shells	Acetamiprid	22 ± 2	-	86.10	1158.70	0.0743	[85]
Eucalyptus wood	Methomyl	25	10–200	32.42	4.02	8.065	This work
H ₃ P ₄ -cotton stalks	Methomyl	25	-	72.85	1600.00	0.0455	[86]
Carbon xerogel	Methomyl	25	20–100	15.2	212.20	0.0716	[87]

Notably, the surface areas of those clays are higher than that of the BC. Interestingly, the adsorption capacity of methomyl over BC is higher than that of carbon xerogel, as it has *ca.* 50-fold of the BC surface area. It is worth noting that the adsorption capacity per unit surface area of the BC for three pesticide removal in our study is also higher than the reported activated biochar materials produced from agricultural waste. Previous work suggested that biochar with a small surface area could provide a high adsorption capacity per unit surface area for pesticide removal because the three-dimensional swelling of biochar occurs in an aqueous environment, and the adsorbates are adsorbed and imbibed at the adsorption sites [40]. Thus, the low-cost and woodchip derived biochar in this work has shown great promise as an effective sorbent for aqueous pesticide removal. It is highly

possible that well-controlled surface functionalization or activation of the biochar materials would further enhance the adsorption capacity of emerging pollutants in wastewater.

4. Conclusions

Woodchip derived biochar material has been applied as a sorbent to remove imidacloprid, acetamiprid, or methomyl from water. The maximum adsorption capacities of pesticides on the biochar can be described in the order of highest to lowest from methomyl to imidacloprid to acetamiprid. Evidence has suggested that the polar functional groups on the biochar surface (hydroxyl and carboxyl groups), and π - π interactions between the pesticides and aromatic carbons in the biochar could be responsible for the high adsorption capacity of the pesticide on the solid sorbent. The chemisorption processes obeyed the pseudo-second order model, and the film-diffusion was the main rate-limiting step for the adsorption of all pesticides in the aqueous media. The adsorption isotherms on the biochar were better described by the Langmuir model for acetamiprid and methomyl, whereas the Freundlich model is fitted well with the imidacloprid adsorption data. Further improvement of the adsorption capacity of pesticides on the biochar may be carried out by conducting surface functionalization of the solid sorbent. However, the functionalization method may increase the production cost of the modified biochar, hence it is impractical for large scale utilization such as in wastewater treatment plants.

Supplementary Materials: The following supporting information can be downloaded at: <https://www.mdpi.com/article/10.3390/min12050528/s1>, Figure S1. Dubini–Redushkevich adsorption isotherms for (a) imidacloprid, (b) acetamiprid and (c) methomyl on BC, respectively; Table S1. Dubinin–Radushkevich and Temkin isotherm parameters for imidacloprid, acetamiprid and methomyl on BC. References [88,89] are cited in the supplementary materials.

Author Contributions: Conceptualization, A.S. and S.M.S.; methodology, A.S. and S.M.S.; formal analysis, A.S.; resources, T.K. and S.M.S.; data curation, A.S. and W.C.; writing-original draft preparation, A.S. and W.C.; writing-review and editing, S.M.S.; visualization, A.S. and W.C.; supervision, S.M.S.; project administration, S.M.S.; funding acquisition, P.K. All authors have read and agreed to the published version of the manuscript.

Funding: This research was funded by National Higher Education Science Research and Innovation Policy Council (NXPO) Contract No. C16F630255, and National Research Council of Thailand under the International Research Network-Green Technologies Network for Sustainable Environment: Food-Water-Energy Nexus (Grants no. IRN62W0005).

Data Availability Statement: Data are contained within the article or Supplementary Material.

Acknowledgments: We thank Mahidol University-Frontier Research Facility (MU-FRF) for instrument support, and the MU-FRF scientists, Nawapol Udpuay and Suwilai Chaveanghong, for their kind assistance in Raman measurements.

Conflicts of Interest: The authors declare no conflict of interest.

References

1. Mojiri, A.; Zhou, J.L.; Robinson, B.; Ohashi, A.; Ozaki, N.; Kindaichi, T.; Farraji, H.; Vakili, M. Pesticides in aquatic environments and their removal by adsorption methods. *Chemosphere* **2020**, *253*, 126646. [[CrossRef](#)] [[PubMed](#)]
2. Agrawal, A.; Pandey, R.; Sharma, B. Water Pollution with Special Reference to Pesticide Contamination in India. *J. Water Resource Prot.* **2010**, *2*, 432–448. [[CrossRef](#)]
3. Meijide, J.; Rodríguez, S.; Sanromán, M.A.; Pazos, M. Comprehensive solution for acetamiprid degradation: Combined electro-Fenton and adsorption process. *J. Electroanal. Chem.* **2018**, *808*, 446–454. [[CrossRef](#)]
4. Meng, S.L.; Chen, J.Z.; Hu, G.H.; Song, C.; Fan, L.M.; Qiu, L.P.; Xu, P. Effects of chronic exposure of methomyl on the antioxidant system in liver of Nile tilapia (*Oreochromis niloticus*). *Ecotoxicol. Environ. Saf.* **2014**, *101*, 1–6. [[CrossRef](#)] [[PubMed](#)]
5. Anderson, T.A.; Salice, C.J.; Erickson, R.A.; McMurry, S.T.; Cox, S.B.; Smith, L.M. Effects of landuse and precipitation on pesticides and water quality in playa lakes of the southern high plains. *Chemosphere* **2013**, *92*, 84–90. [[CrossRef](#)]
6. Van Dijk, T.C.; Van Staaldunen, M.A.; Van der Sluijs, J.P. Macro-Invertebrate Decline in surface water polluted with imidacloprid. *PLoS ONE* **2013**, *8*, e62374. [[CrossRef](#)] [[PubMed](#)]

7. Barbosa, M.O.; Moreira, N.F.F.; Ribeiro, A.R.; Pereira, M.F.R.; Silva, A.M.T. Occurrence and removal of organic micropollutants: An overview of the watch list of EU Decision 2015/495. *Water Res.* **2016**, *94*, 257–279. [[CrossRef](#)]
8. Zhang, C.; Yang, Z.; Jin, W.; Wang, X.; Zhang, Y.; Zhu, S.; Yu, X.; Hu, G.; Hong, Q. Degradation of methomyl by the combination of *Aminobacter* sp. MDW-2 and *Afiplia* sp. MDW-3. *Lett. Appl. Microbiol.* **2017**, *64*, 289–296. [[CrossRef](#)]
9. Zoumenou, B.G.Y.M.; Aïna, M.P.; Imorou Toko, I.; Igout, A.; Douny, C.; Brose, F.; Schiffers, B.; Gouda, I.; Chabi Sika, K.; Kestemont, P.; et al. Occurrence of Acetamiprid Residues in Water Reservoirs in the Cotton Basin of Northern Benin. *Bull. Environ. Contam. Toxicol.* **2019**, *102*, 7–12. [[CrossRef](#)]
10. Starner, K.; Goh, K.S. Detections of the neonicotinoid insecticide imidacloprid in surface waters of three agricultural regions of California, USA, 2010–2011. *Bull. Environ. Contam. Toxicol.* **2012**, *88*, 316–321. [[CrossRef](#)]
11. Goulson, D. An overview of the environmental risks posed by neonicotinoid insecticides. *J. Appl. Ecol.* **2013**, *50*, 977–987. [[CrossRef](#)]
12. Farré, M.; Fernandez, J.; Paez, M.; Granada, L.; Barba, L.; Gutierrez, H.; Pulgarin, C.; Barceló, D. Analysis and toxicity of methomyl and ametryn after biodegradation. *Anal. Bioanal. Chem.* **2002**, *373*, 704–709. [[CrossRef](#)] [[PubMed](#)]
13. Cid Andres, P.A.; Del Mundo, F.R.; Espino, M.P.B. A modified analytical procedure for the determination of carbaryl, carbofuran and methomyl residues in agricultural soil and river water samples from La Trinidad, Benguet and Aurora, Isabela, Philippines. *Philipp. Agric. Sci.* **2006**, *89*, 71–84.
14. Fan, C.; Horng, C.-Y.; Li, S.-J. Structural characterization of natural organic matter and its impact on methomyl removal efficiency in Fenton process. *Chemosphere* **2013**, *93*, 178–183. [[CrossRef](#)] [[PubMed](#)]
15. Pietrzak, D.; Kania, J.; Kmiecik, E.; Malina, G.; Wator, K. Fate of selected neonicotinoid insecticides in soil–water systems: Current state of the art and knowledge gaps. *Chemosphere* **2020**, *255*, 126981. [[CrossRef](#)] [[PubMed](#)]
16. Shamsollahi, Z.; Partovinia, A. Recent advances on pollutants removal by rice husk as a bio-based adsorbent: A critical review. *J. Environ. Manag.* **2019**, *246*, 314–323. [[CrossRef](#)]
17. Bakouri, H.E.; Morillo, J.; Usero, J.; Ouassini, A. Natural attenuation of pesticide water contamination by using ecological adsorbents: Application for chlorinated pesticides included in European Water Framework Directive. *J. Hydrol.* **2009**, *364*, 175–181. [[CrossRef](#)]
18. Carrizosa, M.J.; Calderón, M.J.; Hermosín, M.C.; Cornejo, J. Organosmectites as sorbent and carrier of the herbicide bentazone. *Sci. Total Environ.* **2000**, *247*, 285–293. [[CrossRef](#)]
19. Sudhakar, Y.; Dikshit, A.K. Adsorbent selection for endosulfan removal from water environment. *J. Environ. Sci. Health B* **1999**, *34*, 97–118. [[CrossRef](#)]
20. Taha, S.M.; Amer, M.E.; Elmarsafy, A.E.; Elkady, M.Y. Adsorption of 15 different pesticides on untreated and phosphoric acid treated biochar and charcoal from water. *J. Environ. Chem. Eng.* **2014**, *2*, 2013–2025. [[CrossRef](#)]
21. Ranguin, R.; Jean-Marius, C.; Yacou, C.; Gaspard, S.; Feidt, C.; Rychen, G.; Delannoy, M. Reduction of chlordecone environmental availability by soil amendment of biochars and activated carbons from lignocellulosic biomass. *Environ. Sci. Pollut. Res.* **2020**, *27*, 41093–41104. [[CrossRef](#)] [[PubMed](#)]
22. Mandal, A.; Singh, N.; Purakayastha, T.J. Characterization of pesticide sorption behaviour of slow pyrolysis biochars as lowcost adsorbent for atrazine and imidacloprid removal. *Sci. Total Environ.* **2017**, *577*, 376–385. [[CrossRef](#)] [[PubMed](#)]
23. Yoon, J.-Y.; Kim, J.E.; Song, H.J.; Oh, K.B.; Jo, J.W.; Yang, Y.-H.; Lee, S.H.; Kang, G.; Kim, H.J.; Choi, Y.-K. Assessment of adsorptive behaviors and properties of grape pomace-derived biochar as adsorbent for removal of cymoxanil pesticide. *Environ. Technol. Innov.* **2021**, *21*, 101242. [[CrossRef](#)]
24. Binh, Q.A.; Kajitvichyanukul, P. Adsorption mechanism of dichlorvos onto coconut fibre biochar: The significant dependence of H-bonding and the pore-filling mechanism. *Water Sci. Technol.* **2019**, *79*, 866–876. [[CrossRef](#)]
25. Baharum, N.A.; Nasir, H.M.; Ishak, M.Y.; Isa, N.M.; Hassan, M.A.; Aris, A.Z. Highly efficient removal of diazinon pesticide from aqueous solutions by using coconut shell-modified biochar. *Arab. J. Chem.* **2020**, *13*, 6106–6121. [[CrossRef](#)]
26. Liu, N.; Charrua, A.B.; Weng, C.-H.; Yuan, X.; Ding, F. Characterization of biochars derived from agriculture wastes and their adsorptive removal of atrazine from aqueous solution: A comparative study. *Bioresour. Technol.* **2015**, *198*, 55–62. [[CrossRef](#)]
27. Onsree, T.; Tippayawong, N.; Zheng, A.; Li, H. Pyrolysis behavior and kinetics of corn residue pellets and eucalyptus wood chips in a macro thermogravimetric analyzer. *Case Stud. Therm. Eng.* **2018**, *12*, 546–556. [[CrossRef](#)]
28. Mishra, V.; Sureshkumar, M.K.; Gupta, N.; Kaushik, C.P. Study on Sorption Characteristics of Uranium onto Biochar Derived from Eucalyptus Wood. *Water Air Soil Pollut.* **2017**, *228*, 309. [[CrossRef](#)]
29. Zeng, H.; Zeng, H.; Zhang, H.; Shahab, A.; Zhang, K.; Lu, Y.; Nabi, I.; Naseem, F.; Ullah, H. Efficient adsorption of Cr (VI) from aqueous environments by phosphoric acid activated eucalyptus biochar. *J. Clean. Prod.* **2021**, *286*, 124964. [[CrossRef](#)]
30. Fuentes, A.L.B.; Barraqué, F.; Mercader, R.C.; Scian, A.N.; Montes, M.L. Efficient low-cost magnetic composite based on eucalyptus wood biochar for arsenic removal from groundwater. *Groundw. Sustain. Dev.* **2021**, *14*, 100585. [[CrossRef](#)]
31. Dai, W.; Xu, M.; Zhao, Z.; Zheng, J.; Huang, F.; Wang, H.; Liu, C.; Xiao, R. Characteristics and quantification of mechanisms of Cd²⁺ adsorption by biochars derived from three different plant-based biomass. *Arab. J. Chem.* **2021**, *14*, 103119.
32. Shafiq, M.; Alazba, A.A.; Amin, M.T. Kinetic and isotherm studies of Ni²⁺ and Pb²⁺ adsorption from synthetic wastewater using *Eucalyptus camdulensis*—Derived biochar. *Sustainability* **2021**, *13*, 3785. [[CrossRef](#)]

33. Fernandes, M.J.; Moreira, M.M.; Paíga, P.; Dias, D.; Bernardo, M.; Carvalho, M.; Lapa, N.; Fonseca, I.; Morais, S.; Figueiredo, S.; et al. Evaluation of the adsorption potential of biochars prepared from forest and agri-food wastes for the removal of fluoxetine. *Bioresour. Technol.* **2019**, *292*, 121973. [[PubMed](#)]
34. Singh, B.K.; Rawat, N.S. Comparative sorption kinetic studies of phenolic compounds on fly ash and impregnated fly ash. *J. Chem. Technol. Biotechnol.* **1994**, *61*, 57–65. [[CrossRef](#)]
35. Amin, N.K. Removal of direct blue-106 dye from aqueous solution using new activated carbons developed from pomegranate peel: Adsorption equilibrium and kinetics. *J. Hazard. Mater.* **2009**, *165*, 52–62. [[CrossRef](#)]
36. Ahmed, M.J.; Dhedan, S.K. Equilibrium isotherms and kinetics modeling of methylene blue adsorption on agricultural wastes-based activated carbons. *Fluid Ph. Equilibria* **2012**, *317*, 9–14.
37. Essandoh, M.; Wolgemuth, D.; Pittman, C.U.; Mohan, D.; Mlsa, T. Adsorption of metribuzin from aqueous solution using magnetic and nonmagnetic sustainable low-cost biochar adsorbents. *Environ. Sci. Pollut. Res.* **2017**, *24*, 4577–4590. [[CrossRef](#)]
38. Cárdenas, L.J.; Giraldo, L.; Moreno-Piraján, J.C. Physicochemical characterization of santa barbara amorphous-15 (SBA-15) and its functionalization with polyaniline for phenol adsorption. *Processes* **2022**, *10*, 188. [[CrossRef](#)]
39. Chaves Fernandes, B.C.; Ferreira Mendes, K.; Dias Júnior, A.F.; da Silva Caldeira, V.P.; da Silva Teófilo, T.M.; Severo Silva, T.; Mendonça, V.; de Freitas Souza, M.; Valadão Silva, D. Impact of Pyrolysis Temperature on the Properties of Eucalyptus Wood-Derived Biochar. *Materials* **2020**, *13*, 5841.
40. Fernandes, B.C.C.; Mendes, K.F.; Tornisielo, V.L.; Teófilo, T.M.S.; Takeshita, V.; das Chagas, P.S.F.; Lins, H.A.; Souza, M.F.; Silva, D.V. Effect of pyrolysis temperature on eucalyptus wood residues biochar on availability and transport of hexazinone in soil. *Int. J. Environ. Sci. Technol.* **2021**. [[CrossRef](#)]
41. Essandoh, M.; Wolgemuth, D.; Pittman, C.U.; Mohan, D.; Mlsna, T. Phenoxy herbicide removal from aqueous solutions using fast pyrolysis switchgrass biochar. *Chemosphere* **2017**, *174*, 49–57. [[CrossRef](#)] [[PubMed](#)]
42. Keiluweit, M.; Nico, P.S.; Johnson, M.G.; Kleber, M. Dynamic molecular structure of plant biomass-derived black carbon (biochar). *Environ. Sci. Technol.* **2010**, *44*, 1247–1253. [[CrossRef](#)] [[PubMed](#)]
43. Mayakaduwa, S.S.; Vithanage, M.; Karunarathna, A.; Mohan, D.; Ok, Y.S. Interface interactions between insecticide carbofuran and tea waste biochars produced at different pyrolysis temperatures. *Chem. Speciat. Bioavailab.* **2016**, *28*, 110–118. [[CrossRef](#)]
44. Oh, S.-Y.; Son, J.-G.; Chiu, P.C. Biochar-mediated reductive transformation of nitro herbicides and explosives. *Environ. Toxicol. Chem.* **2013**, *32*, 501–508. [[CrossRef](#)]
45. Zheng, W.; Guo, M.; Chow, T.; Bennett, D.N.; Rajagopalan, N. Sorption properties of greenwaste biochar for two triazine pesticides. *J. Hazard. Mater.* **2010**, *181*, 121–126. [[CrossRef](#)] [[PubMed](#)]
46. Maziarka, P.; Wurzer, C.; Arauzo, P.J.; Dieguez-Alonso, A.; Mašek, O.; Ronsse, F. Do you BET on routine? The reliability of N₂ physisorption for the quantitative assessment of biochar's surface area. *Chem. Eng. J.* **2021**, *418*, 129234. [[CrossRef](#)]
47. Sing, K.S.W.; Rouquerol, F.; Rouquerol, J.; Llewellyn, P.; Rouquerol, F.; Rouquerol, J.; Sing, K.S.W.; Llewellyn, P.; Maurin, G. (Eds.) *Adsorption by Powders and Porous Solids*, 2nd ed.; Academic Press: Cambridge, MA, USA, 2013; pp. 269–302.
48. Suo, F.; You, X.; Ma, Y.; Li, Y. Rapid removal of triazine pesticides by P doped biochar and the adsorption mechanism. *Chemosphere* **2019**, *235*, 918–925. [[CrossRef](#)]
49. Tsai, W.T.; Chen, H.R. Adsorption kinetics of herbicide paraquat in aqueous solution onto a low-cost adsorbent, swine-manure-derived biochar. *Int. J. Environ. Sci. Technol.* **2013**, *10*, 1349–1356. [[CrossRef](#)]
50. ICDD. *ICDD Powder Diffraction File Inorganic and Organic Data Book International Centre for Diffraction Data*; ICDD: Newtown Square, PA, USA, 2010.
51. Singh, B.; Raven, M.D.X.; Singh, B.; Camps-Arbestain, M.; Lehmann, J. (Eds.) *Biochar A Guide to Analytical Methods*; CSIRO Publishing: Collingwood, VIC, Australia, 2017; pp. 245–252.
52. Limwikran, T.; Kheoruenromne, I.; Suddhiprakarn, A.; Prakongkep, N.; Gilkes, R.J. Dissolution of K, Ca, and P from biochar grains in tropical soils. *Geoderma* **2018**, *312*, 139–150. [[CrossRef](#)]
53. Yuan, J.-H.; Xu, R.-K.; Zhang, H. The forms of alkalis in the biochar produced from crop residues at different temperatures. *Bioresour. Technol.* **2011**, *102*, 3488–3497. [[CrossRef](#)]
54. Dehkoda, A.M.; Ellis, N.; Gyenge, E. Effect of activated biochar porous structure on the capacitive deionization of NaCl and ZnCl₂ solutions. *Microporous Mesoporous Mater.* **2016**, *224*, 3488–3497. [[CrossRef](#)]
55. Ocampo-Perez, R.; Padilla-Ortega, E.; Medellín-Castillo, N.A.; Coronado-Oyarvide, P.; Aguilar-Madera, C.G.; Segovia-Sandoval, S.J.; Flores-Ramírez, R.; Parra-Marfil, A. Synthesis of biochar from chili seeds and its application to remove ibuprofen from water. Equilibrium and 3D modeling. *Sci. Total Environ.* **2019**, *655*, 1397–1408. [[CrossRef](#)] [[PubMed](#)]
56. Ferrari, A.C.; Robertson, J. Interpretation of Raman spectra of disordered and amorphous carbon. *Phys. Rev. B* **2000**, *61*, 14095. [[CrossRef](#)]
57. Pelle, F.D.; Battista, R.D.; Vázquez, L.; Palomares, F.J.; Del Carlo, M.; Sergi, M.; Compagnone, D.; Escarpa, A. Press-transferred carbon black nanoparticles for class-selective antioxidant electrochemical detection. *Appl. Mater. Today* **2017**, *9*, 29–36. [[CrossRef](#)]
58. Chen, B.; Zhou, D.; Zhu, L. Transitional adsorption and partition of nonpolar and polar aromatic contaminants by biochars of pine needles with different pyrolytic temperatures. *Environ. Sci. Technol.* **2008**, *42*, 5137–5143. [[CrossRef](#)]
59. Sobik-Szołtysek, J.; Wystalska, K.; Malińska, K.; Meers, E. Influence of Pyrolysis Temperature on the Heavy Metal Sorption Capacity of Biochar from Poultry Manure. *Materials* **2021**, *14*, 6566. [[CrossRef](#)]

60. Wu, W.; Yang, M.; Feng, Q.; McGrouther, K.; Wang, H.; Lu, H.; Chen, Y. Chemical characterization of rice straw-derived biochar for soil amendment. *Biomass Bioenergy* **2012**, *47*, 268–276. [[CrossRef](#)]
61. Leng, L.; Yuan, X.; Zeng, G.; Shao, J.; Chen, X.; Wu, Z.; Wang, H.; Peng, X. Surface characterization of rice husk bio-char produced by liquefaction and application for cationic dye (Malachite green) adsorption. *Fuel* **2015**, *155*, 77–85. [[CrossRef](#)]
62. Jacob, M.M.; Ponnuchamy, M.; Kapoor, A.; Sivaraman, P. Bagasse based biochar for the adsorptive removal of chlorpyrifos from contaminated water. *J. Environ. Chem. Eng.* **2020**, *8*, 103904. [[CrossRef](#)]
63. Bootharaju, M.S.; Pradeep, T. Understanding the degradation pathway of the pesticide, chlorpyrifos by noble metal nanoparticles. *Langmuir* **2012**, *28*, 2671–2679. [[CrossRef](#)]
64. Chen, C.; Geng, X.; Huang, W. Adsorption of 4-chlorophenol and aniline by nanosized activated carbons. *Chem. Eng. J.* **2017**, *327*, 941–952. [[CrossRef](#)]
65. Tran, H.N.; You, S.-J.; Hosseini-Bandegharai, A.; Chao, H.-P. Mistakes and inconsistencies regarding adsorption of contaminants from aqueous solutions: A critical review. *Water Res.* **2017**, *120*, 88–116. [[CrossRef](#)] [[PubMed](#)]
66. Wahab, M.A.; Jellali, S.; Jedidi, N. Effect of temperature and pH on the biosorption of ammonium onto *Posidonia oceanica* fibers: Equilibrium, and kinetic modeling studies. *Bioresour. Technol.* **2010**, *101*, 8606–8615. [[CrossRef](#)] [[PubMed](#)]
67. Huang, D.; Wang, X.; Zhang, C.; Zeng, G.; Peng, Z.; Zhou, J.; Cheng, M.; Wang, R.; Hu, Z.; Qin, X. Sorptive removal of ionizable antibiotic sulfamethazine from aqueous solution by graphene oxide-coated biochar nanocomposites: Influencing factors and mechanism. *Chemosphere* **2017**, *186*, 414–421. [[CrossRef](#)] [[PubMed](#)]
68. Elamin, M.R.; Abdulkhair, B.Y.; Algethami, F.K.; Khezami, L. Linear and nonlinear investigations for the adsorption of paracetamol and metformin from water on acid-treated clay. *Sci. Rep.* **2021**, *11*, 13606. [[CrossRef](#)]
69. Salman, J.M.; Njoku, V.O.; Hameed, B.H. Adsorption of pesticides from aqueous solution onto banana stalk activated carbon. *Chem. Eng. J.* **2021**, *174*, 41–48. [[CrossRef](#)]
70. Wang, Y.; Zhang, Y.; Li, S.; Zhong, W.; Wei, W. Enhanced methylene blue adsorption onto activated reed-derived biochar by tannic acid. *J. Mol. Liq.* **2018**, *268*, 658–666. [[CrossRef](#)]
71. Srikaow, A.; Butburee, T.; Pon-On, W.; Srihirin, T.; Uraisin, K.; Suttiponpanit, K.; Chaveanghong, S.; Smith, S.M. Efficient mercury removal at ultralow metal concentrations by cysteine functionalized carbon-coated magnetite. *Appl. Sci.* **2020**, *10*, 8262. [[CrossRef](#)]
72. Ali, I.; AL-Othman, Z.A.; Alwarthan, A. Green synthesis of functionalized iron nano particles and molecular liquid phase adsorption of ametryn from water. *J. Mol. Liq.* **2016**, *221*, 1168–1174. [[CrossRef](#)]
73. Moussavi, G.; Hosseini, H.; Alahabadi, A. The investigation of diazinon pesticide removal from contaminated water by adsorption onto NH₄Cl-induced activated carbon. *Chem. Eng. J.* **2013**, *214*, 172–179. [[CrossRef](#)]
74. Wang, F.; Sun, W.; Pan, W.; Xu, N. Adsorption of sulfamethoxazole and 17 β -estradiol by carbon nanotubes/CoFe₂O₄ composites. *Chem. Eng. J.* **2015**, *274*, 17–29. [[CrossRef](#)]
75. Gordon, M.S.; Mullin, J.M.; Pruitt, S.R.; Roskop, L.B.; Slipchenko, L.V.; Boatz, J.A. Accurate Methods for Large Molecular Systems. *J. Phys. Chem. B* **2009**, *113*, 9646–9663. [[CrossRef](#)] [[PubMed](#)]
76. Inyang, M.; Dickerson, E. The potential role of biochar in the removal of organic and microbial contaminants from potable and reuse water: A review. *Chemosphere* **2015**, *134*, 232–240. [[CrossRef](#)] [[PubMed](#)]
77. Pandith, A.; Hazra, G.; Kim, H.-S. A new fluorogenic sensing platform for salicylic acid derivatives based on π - π and NH- π interactions between electron-deficient and electron-rich aromatics. *Spectrochim. Acta A Mol. Biomol. Spectrosc.* **2017**, *178*, 151–159. [[CrossRef](#)]
78. Yavari, S.; Malakahmad, A.; Sapari, N.B. Biochar efficiency in pesticides sorption as a function of production variables—a review. *Environ. Sci. Pollut. Res.* **2015**, *22*, 13824–13841. [[CrossRef](#)]
79. Caban, M.; Folentarska, A.; Lis, H.; Kobylis, P.; Kumirska, J.; Stepnowski, P.; Ciesielski, W. Valuable polar moieties on cereal-derived biochars. *Colloids Surf. A Physicochem. Eng. Asp.* **2019**, *561*, 275–282. [[CrossRef](#)]
80. Choumane, F.Z.; Benguella, B. Removal of acetamiprid from aqueous solutions with low-cost sorbents. *Desalination Water Treat.* **2016**, *57*, 419–430. [[CrossRef](#)]
81. Zhao, R.; Ma, X.; Xu, J.; Zhang, Q. Removal of the pesticide imidacloprid from aqueous solution by biochar derived from peanut shell. *Bioresources* **2018**, *13*, 5656–5669.
82. Ma, Y.; Qi, Y.; Yang, L.; Wu, L.; Li, P.; Gao, F.; Qi, X.; Zhang, Z. Adsorptive removal of imidacloprid by potassium hydroxide activated magnetic sugarcane bagasse biochar: Adsorption efficiency, mechanism and regeneration. *J. Clean. Prod.* **2021**, *292*, 126005. [[CrossRef](#)]
83. Ma, Y.; Chen, S.; Qi, Y.; Yang, L.; Wu, L.; He, L.; Li, P.; Qi, X.; Gao, F.; Ding, Y.; et al. An efficient, green and sustainable potassium hydroxide activated magnetic corn cob biochar for imidacloprid removal. *Chemosphere* **2021**, *291*, 132707. [[CrossRef](#)]
84. Mohammad, S.G.; Ahmed, S.M.; Amr, A.E.-G.E.; Kamel, A.H. Porous activated carbon from lignocellulosic agricultural waste for the removal of acetamiprid pesticide from aqueous solutions. *Molecules* **2020**, *25*, 2339. [[CrossRef](#)] [[PubMed](#)]
85. Dolatabadi, M.; Naidu, H.; Ahmadzadeh, S. A green approach to remove acetamiprid insecticide using pistachio shell-based modified activated carbon; economical groundwater treatment. *J. Clean. Prod.* **2021**, *316*, 128226. [[CrossRef](#)]
86. El-Geundi, M.S.; Nassar, M.M.; Farrag, T.E.; Ahmed, M.H. Methomyl Adsorption onto Cotton Stalks Activated Carbon (CSAC): Equilibrium and Process Design. *Procedia Environ. Sci. Eng. Manag.* **2013**, *17*, 630–639. [[CrossRef](#)]

-
87. Fathy, N.A.; Attia, A.A.; Hegazi, B. Nanostructured activated carbon xerogels for removal of methomyl pesticide. *Desalination Water Treat.* **2016**, *57*, 9957–9970. [[CrossRef](#)]
 88. Foo, K.Y.; Hameed, B.H. Insights into the modeling of adsorption isotherm systems. *Chem. Eng. J.* **2010**, *156*, 2–10. [[CrossRef](#)]
 89. Mohammad, S.G.; Ahmed, S.M.; Badawi, A.F.M. A comparative adsorption study with different agricultural waste adsorbents for removal of oxamyl pesticide. *Desalin. Water Treat.* **2015**, *55*, 2109–2120. [[CrossRef](#)]